Hybridization-Controlled Pseudogap State in the Quantum Critical Superconductor $CeCoIn_5$

Harim Jang,[1] Vuong Thi Anh Hong,[1] Jihyun Kim,[1] Xin Lu,[2] and Tuson Park[1,3,*]
[1]Department of Physics, Sungkyunkwan University, Suwon 16419, Republic of Korea
[2]Center for Correlated Matter and Department of Physics, Zhejiang University, Hangzhou 310058, China
[3]Center for Quantum Materials and Superconductivity (CQMS), Sungkyunkwan University, Suwon 16419, Republic of Korea

(Received 16 July 2022; accepted 23 January 2023; published 16 February 2023)

The origin of the partial suppression of the electronic density states in the enigmatic pseudogap behavior, which is at the core of understanding high-T_c superconductivity, has been hotly contested as either a hallmark of preformed Cooper pairs or an incipient order of competing interactions nearby. Here, we report the quasiparticle scattering spectroscopy of the quantum critical superconductor $CeCoIn_5$, where a pseudogap with energy Δ_g was manifested as a dip in the differential conductance (dI/dV) below the characteristic temperature of T_g. When subjected to external pressure, T_g and Δ_g gradually increase, following the trend of increase in quantum entangled hybridization between the Ce $4f$ moment and conduction electrons. On the other hand, the superconducting (SC) energy gap and its phase transition temperature shows a maximum, revealing a dome shape under pressure. The disparate dependence on pressure between the two quantum states shows that the pseudogap is less likely involved in the formation of SC Cooper pairs, but rather is controlled by Kondo hybridization, indicating that a novel type of pseudogap is realized in $CeCoIn_5$.

DOI: 10.1103/PhysRevLett.130.076301

The pseudogap, reminiscent of the energy gap from the depression of the density of states or a partial gap near the Fermi level, is of great interest because of its potential connection to the intertwined quantum states emergent in strongly correlated systems [1–8]. Attractive, yet puzzling, is the observation of the pseudogap in various unconventional superconductors, indicating that understanding its microscopic origin is crucial to resolving the mysteries of high-temperature superconductivity [4,9–13]. Although extensive studies have been conducted to elucidate the origin of the pseudogap, its relationship with unconventional superconductivity is still controversial owing to the disorder inherent in chemical substitution, close proximity to other intertwined quantum states, and large thermal fluctuations [3,6,7,14].

In the prototypical unconventional superconductor $CeCoIn_5$, which is located near a quantum critical point in its stoichiometric form, a pseudogap feature in the normal state above the superconducting transition temperature (T_c) has been reported from spectroscopic and transport measurements [9,15–17]. The precursor state of Cooper pairs was proposed as the origin of a pseudogap from scanning tunneling spectroscopy (STS) measurements, where depletion in the differential conductance (dI/dV) near the Fermi level was observed below 3.0 K with an energy scale of 1 meV [15]. Deviating from the T-linear non-Fermi liquid behavior, the electrical resistivity was suppressed below 3 K, which was ascribed to a decrease in the scattering rate owing to the preformed Cooper pairs [16]. In contrast, the close proximity to the antiferromagnetic quantum critical point (AFM QCP) of $CeCoIn_5$ suggests that a new form of competing orders may be realized in the normal state, requiring further study on the nature of the pseudogap in $CeCoIn_5$ [7,16,18].

Here, we report the hybridization-controlled novel pseudogap state in the quantum critical superconductor $CeCoIn_5$. A dip overlaid with the Fano-resonance line in differential conductance dI/dV is observed via quasiparticle scattering spectroscopy (QSS) at temperatures higher than T_c, indicating the appearance of a pseudogap with energy Δ_g in the normal state. In stark contrast to the dome-shape pressure dependence of the superconducting (SC) transition temperature, Δ_g and its emerging temperature (T_g) monotonically increase under pressure and follow the trend of the transport Kondo coherence temperature (T_{coh}). The Fano-resonance asymmetry in dI/dV under pressure increases with decreasing temperature and reveals a scaling behavior against the reduced temperature (T/T_{sat}) in the high-temperature regime, signifying that T_{sat} is the onset of Kondo lattice coherence. With a further decrease in temperature, it deviates from the scaling and shows a peak or kink at T_{max}. When plotted together with pressure, the characteristic temperatures of T_g, T_{max}, and T_{coh} follow the same pressure dependence with the pseudogap energy Δ_g, but is different from that of T_c. These discoveries reveal that the nature of the pseudogap in $CeCoIn_5$ is not related to

formation of Cooper electron pairs, but is pertinent to Kondo hybridization.

Figure 1(a) shows the generic temperature-pressure phase diagram of $CeCoIn_5$, where T_c peaked at 1.5 GPa shows a dome shape and the transport Kondo coherence temperature determined from the resistivity maximum monotonically increases under pressure [16,19]. The dashed line is the projected pseudogap temperature based on a preformed Cooper pair scenario, which decreases under pressure and disappears near the end of the SC dome [16]. The inset shows a schematic view of the point-contact junction surrounded by a pressure medium; see the Supplemental Material for the details [20]. In QSS obtained from the point-contact technique, two distinct paths of the transmitting electrons to heavy-fermion metal are considered: tunneling into the conduction band (c channel) and the heavy-electron band (f channel) [34–36]. Quantum interference between these two paths produces the Fano line in dI/dV with a peak centered at the Kondo resonance energy (ε), which can be described by the generalized Fano resonance model for the Kondo lattice [34]:

$$\frac{dI}{dV}(V,T) = g_0 + g_I \int \frac{df(E-V,T)}{dV}\frac{|q-\tilde{E}|^2}{1+\tilde{E}^2}dE \quad (1)$$

The term $|q-\tilde{E}|^2/1+\tilde{E}^2$ represents the simple Fano line, where $\tilde{E} = (E-\varepsilon)/[(aV)^2+\gamma^2]^{1/2}$ is a phenomenologically modified expression. The Fano parameter $q = q_1 + iq_2$ reflects the tunneling ratio between the two paths. Here, q_2 describes the direct tunneling into the $c-f$ coupled state around ε without interference, which could lead to the destruction of the Fano interference. The variables $f(E,T)$, g_0, and γ are the Fermi function, background conductance, and scattering rate at the zero-bias voltage within the f channel, respectively (see Sec. C in the Supplemental Material for more details [20]).

The temperature evolution of dI/dV for $CeCoIn_5$ at ambient pressure is selectively displayed from 70 (top) to 1.5 K (bottom) with a rigid offset for clarity in Fig. 1(b). The two-peak structure with spacing of ~2.4 meV at 1.5 K is ascribed to the Andreev reflection (AR), which is the hallmark of superconductivity [37]. At temperatures above T_c of 2.3 K, the AR is completely suppressed, whereas a dip feature in dI/dV is observed near zero-bias voltage, as indicated by the arrow at 3.0 K. The solid lines are the best fit of the Fano resonance model, showing good agreement with the experimental data (see Fig. S3, S7, and S8 in the Supplemental Material for the detailed analysis for the full range of pressure and temperature [20]). The Kondo resonance peak near $\varepsilon = 3.05$ meV is gradually suppressed as the temperature increases, and is hardly noticeable at temperatures above $T_{\mathrm{coh}} \sim 45$ K, which is consistent with previous results [34,38]. In contrast, the asymmetry in dI/dV still holds even at 70 K.

The differential conductance of $CeCoIn_5$ divided by the Fano contribution, $dI/dV/dI/dV|_{\mathrm{FANO}}$, is plotted for several temperatures with an offset for clarity in Fig. 2(a), where the evolution of the dip feature as a function of

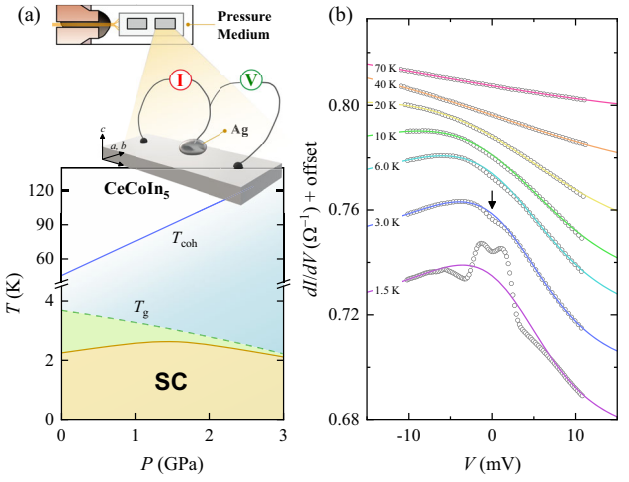

FIG. 1. (a) Generic $P-T$ phase diagram of $CeCoIn_5$. The green dashed line is a pseudogap boundary predicted from previous works [16]. The inset shows the schematic view for the quasiparticle scattering spectroscopy under pressure, where the junction is made on the $a-b$ crystallographic plane. (b) Differential conductance (dI/dV) of $CeCoIn_5$ at representative temperatures and at ambient pressure. The solid lines are the best fits using the Fano resonance model (see the main text for details). The arrow at 3.0 K indicates a dip feature near the zero-bias voltage. All the curves are rigidly shifted for clarity.

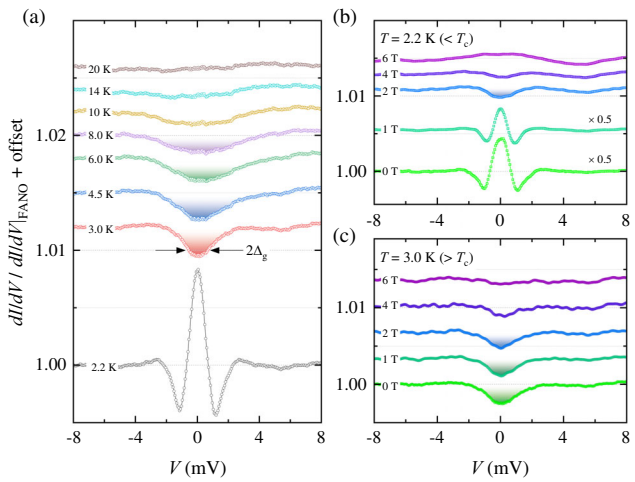

FIG. 2. (a) Temperature-dependent normalized differential conductance, $dI/dV/dI/dV|_{\mathrm{FANO}}$, at ambient pressure, where $dI/dV|_{\mathrm{FANO}}$ is the best fit of the Fano resonance model. The dependences on the magnetic field of $dI/dV/dI/dV|_{\mathrm{FANO}}$ at 2.2 and 3.0 K are plotted in (b) and (c), respectively. The shaded area highlights the minimum near the zero-bias voltage. For clarity, all the curves are rigidly shifted against the bottom curves of 2.2 K, 0 T, and 0 T for panel (a), (b), and (c), respectively. In (c), the spectra at 0 and 1 T are multiplied by a factor of 0.5 for comparison.

temperature is highlighted by the color shades (see Fig. S4 in the Supplemental Material for raw data [20]). With increasing temperature, the amplitude of the dip is suppressed and completely smeared out above the characteristic temperature of T_g, whereas the width of the dip (Δ_g) does not decrease as observed in a normal order parameter. The magnetic field dependence of the dip feature in dI/dV of $CeCoIn_5$ at 2.2 and 3.0 K at ambient pressure is summarized in Figs. 2(b) and 2(c), respectively. At 2.2 K, which is slightly below T_c, the AR peak is observed at 0 T and is suppressed under a magnetic field. When the field is larger than the upper critical field, the AR is completely suppressed, but a dip feature is introduced instead. However, at 3.0 K, which is slightly higher than T_c, a dip feature appears, while AR peak is absent. The dip is gradually suppressed with the increasing field and is not apparent above 4.0 T. The energy width Δ_g (~ 0.8 meV), which is determined as the half of the full width at half maximum (FWHM) at just above T_c, is comparable to that of the pseudogap reported in STM on $CeCoIn_5$ [9,15,17]. As increasing temperature, the dip was filled up smoothly and almost independent of temperature, as observed in numerous high-T_c cuprates [39]. These features suggest that the dip in dI/dV arises from the opening of the pseudogap of $CeCoIn_5$ near the Fermi level.

The dependence on temperature at 0 T and magnetic field at 3.0 K of the normalized differential conductance, $dI/dV/dI/dV|_{\mathrm{FANO}}$, are depicted as a color contour plot for representative pressures in Figs. 3(a)–3(e) and Figs. 3(f)–3(j), respectively. The plume shape within the energy gap Δ_g near the zero-bias voltage describes the pseudogap feature, where the pseudogap regime is enlarged with increasing pressure on both the temperature and magnetic field vs. bias voltage planes. The onset temperature T_g is determined using the criteria of -0.2% boundary in $dI/dV/dI/dV|_{\mathrm{FANO}}$ for all pressure ranges (see Fig. S4 in the Supplemental Material for more details [20]). The application of pressure changes the gap feature systematically: T_g of $5.5(\pm 1.0)$ K at 0.00 GPa increases to $12.5(\pm 2.1)$ K at 2.34 GPa, whereas $2\Delta_g$ of $1.60(\pm 0.21)$ meV at 0.00 GPa increases to $3.96(\pm 0.71)$ meV at 2.34 GPa. In addition, the critical field required to destroy the pseudogap feature at 3.0 K increases from 3.0 T at 0.0 GPa to a field higher than 8.0 T at 2.34 GPa (see Fig. S9 and S10 in the Supplemental Material for details [20]). The suppression of the gap amplitude under a magnetic field, as shown in Fig. 3, is different from that of temperature, implying that the magnetic field not only fills the gapped feature, but also suppresses the onset temperature of pseudogap feature.

The degree of Fano asymmetry in dI/dV can be defined by the ratio of the differential conductance value at a specific energy of positive and negative bias [38]. We select

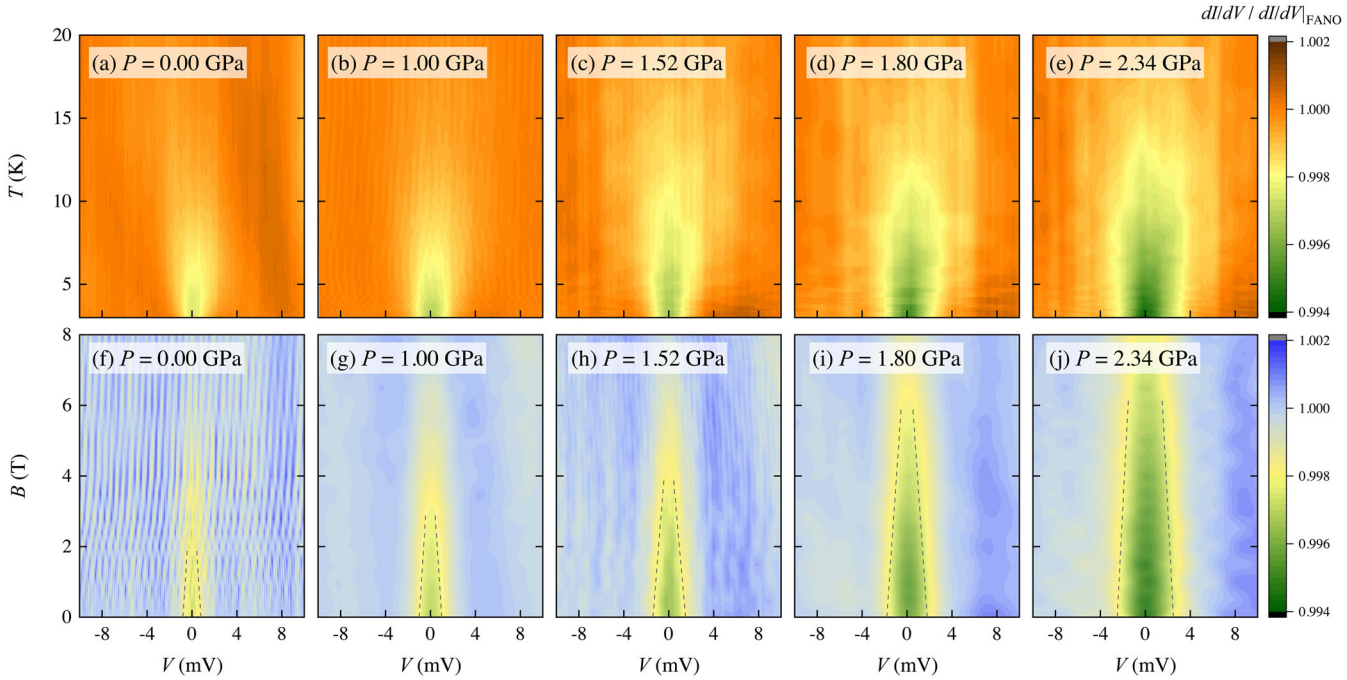

FIG. 3. Color contour plot of $dI/dV/dI/dV|_{\mathrm{FANO}}$ at (a) $P = 0.00$, (b) 1.00, (c) 1.52, (d) 1.80, and (e) 2.34 GPa in the temperature (T) vs bias-voltage (V) axes. Color contour plot of $dI/dV/dI/dV|_{\mathrm{FANO}}$ under magnetic field at 3.0 K and at (f) $P = 0.00$, (g) 1.00, (h) 1.52, (i) 1.80, and (j) 2.34 GPa in the field (B) vs bias-voltage (V) axes. Dark brown and blue in the color scale describe positive values, whereas green represents negatives. All the contour plots are shown with the same scale for comparison and the dashed lines are guides to the eye.

10 mV as a criterion to define the degree of asymmetry, i.e., $A(\%) = 100 \times (dI/dV|_{-10\,\mathrm{mV}} - dI/dV|_{+10\,\mathrm{mV}})/(dI/dV|_{+10\,\mathrm{mV}})$ (see Fig. S10 in the Supplemental Material for the results with different criteria [20]). Because Ce $4f$ electrons are localized at high temperatures, the $c-f$ coupling strength is expected to be suppressed with increasing temperature, resulting in a decrease in A and saturate to zero above the characteristic temperature, T_{sat}. The temperature dependence of $A(T)$ follows the semiphenomenological relation of the two-fluid model, depicted as a dashed line in Fig 4(a) in the high-temperature regime [40]:

$$A(T) \propto \left(1 - \frac{T}{T_{\mathrm{sat}}}\right)^{3/2} \left[1 - \ln\left(\frac{T}{T_{\mathrm{sat}}}\right)\right]. \qquad (2)$$

Here, the first term is an order parameter that characterizes the collective coherent phenomenon, while the second term is the average effective mass of heavy quasiparticle that increases logarithmically. At ambient pressure, the asymptotic temperature T_{sat} is approximately 150 K, which is much higher than the transport coherence temperature $T_{\mathrm{coh}} \sim 45$ K [40–42], but comparable with the onset temperature of the collective $c-f$ hybridization gap reported by angle-resolved photoemission spectroscopy (ARPES) and ultrafast optical spectroscopy [43,44]. In the low-T regime far below T_{sat}, $A(T)$ starts to deviate from the two-fluid description and shows a maximum (or kink) at the characteristic temperature T_{max}, indicated by the arrows in Fig 4(a). We note that such discrepancy between energy-resolved spectroscopy and transport measurement on T_{sat} was also reported in other Kondo lattice $YbRh_2Si_2$ [45].

When subjected to external pressure, the magnitude of Fano asymmetry A decreases in the low-T regime, but collapses onto a single curve in the high-T regime as a function of the reduced temperature of T/T_{sat} for different pressures. As shown in the inset of Fig 4(a), both T_{sat} and T_{max} linearly increase with pressure; this can be ascribed to the enhanced $c-f$ coupling strength. The maximum Fano asymmetry at T_{max} may be used as a possible indicator of the complete transition in a broad crossover from the Kondo incoherent to the entangled quantum coherent state. Supporting this interpretation, ARPES measurements show that the saturating behavior of the f-electron weight occurs near T_{max} (~20 K) in $CeCoIn_5$ [43,44].

Figure 4(b) summarizes the comprehensive $P-T$ phase diagram of $CeCoIn_5$ overlaid with the normalized zero-bias-conductance (ZBC) color contour plot, where the ZBC is normalized to its value at T_c for clarity. The characteristic temperatures of T_g, T_{coh}, T_{max}, $T_{c,\rho}$, and $T_{c,\mathrm{QSS}}$ are plotted on the left ordinate. Here, T_{coh} and T_{max} are multiplied by a factor of 0.1 and 0.3, respectively, for comparison with other temperature scales. The width of the suppressed dI/dV, which is attributed to the opening of a pseudogap

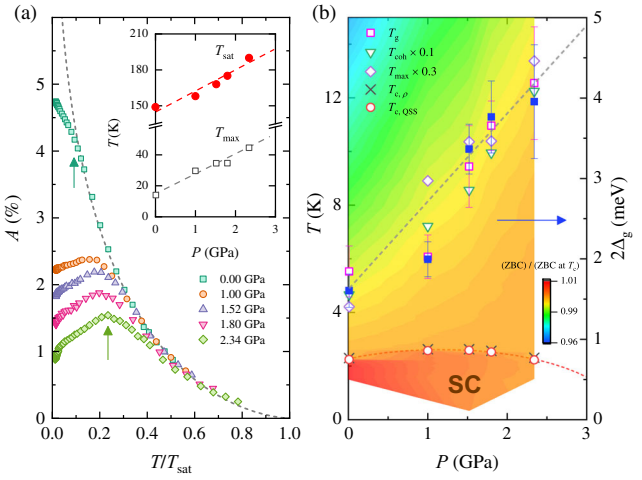

FIG. 4. (a) Fano asymmetry, determined at 10 mV, as a function of reduced temperature, T/T_{sat}. The dashed line is the universal temperature dependence curve estimated from the two-fluid model (see the main text for details). The arrows indicate T_{max}, where $A(T)$ has a maximum or kink. Pressure-dependent T_{sat} and T_{max} are shown in the inset, where the dashed line is a guide to the eye. (b) Comprehensive $P-T$ phase diagram overlaid with the color contour plot of the normalized zero-bias conductance, (ZBC)/(ZBC at T_c). T_g, T_{coh}, T_{max}, $T_{c,\rho}$, and $T_{c,\mathrm{QSS}}$, plotted on the left ordinate, stand for characteristic temperatures for pseudogap, transport Kondo coherence, maximum Fano asymmetry, and SC transition determined from resistivity and QSS, respectively, where T_{coh} and T_{max} are consecutively multiplied by a factor of 0.1 and 0.3 for comparison (see Fig. S14 in the Suppleemntal Material for more details [20]). The pseudogap width $2\Delta_g$ is plotted on the right ordinate. The dashed lines are visual guides. Errors represent uncertainty in determining the characteristic temperatures as well as the pseudogap based on the standard deviation of each definition.

$2\Delta_g$, is plotted on the right ordinate. All the temperature and energy scales that characterize the low-energy physics in the normal state nearly triple as the pressure increases from 1 bar to 2.34 GPa and follow the linear-in-P trend (see the dashed line). The pressure dependences of both T_g and Δ_g, which characterize the pseudogap, deviate significantly from that of T_c, implying that the pseudogap in $CeCoIn_5$ is not involved in the Cooper pair formation process. Instead, the pseudogap temperature and its amplitude closely follow the pressure dependence of T_{coh} (see Fig. S13 in the Supplemental Material [20]), suggesting that the depletion of the density of states in the normal state originates from the collective behavior of $c-f$ hybridization.

In high-T_c cuprates, a pseudogap determined from the depletion in the quasiparticle density of states below T^* ($\gg T_c$) has almost a temperature-independent energy width, and the SC gap-to-T^* ratio ($2\Delta_{SC}/k_{\mathrm{B}}T^*$) is approximately 4.3 for various members of high-T_c cuprates [39]. Similarly, the pseudogap of $CeCoIn_5$ is distinct from the temperature response of the ordinary order parameter and shows filling-up behavior with increasing temperature

(see Fig. 3 and Fig. S5 in the Supplemental Material for more details [20]). The SC gap-to-T_g ratio of $CeCoIn_5$, contrarily, is approximately $2.6(\pm 0.98)$ at ambient pressure, which is substantially smaller than those of high-T_c cuprates. Furthermore, the response to doping concentration (or pressure) is disparate between the two families of unconventional superconductors. With increasing doping level, the onset temperature as well as the size of the pseudogap in the cuprates decrease and disappear at the critical concentration above which the SC phase is suppressed [4,39]. In $CeCoIn_5$, in striking contrast, the pseudogap behavior continuously increases even in the high-pressure regime, where superconductivity is suppressed. These contrasting behaviors against the SC transition temperature indicate that the origin of the pseudogap of $CeCoIn_5$ is different from that of the high-T_c cuprates, emphasizing the importance of more comprehensive tests to elucidate the nature and mechanism of pseudogap phenomena in strongly correlated superconductors.

A few prior spectroscopic studies on $CeCoIn_5$ surface have observed the smooth evolution of SC gap with lowering temperature, suggesting preformed Cooper pairs above T_c [15,46]. Since both the SC gap and pseudogap feature is revealed as a dip structure in the dI/dV probed by tunneling spectroscopic method, it is difficult to determine if the pseudogap behavior is intertwined with the superconductivity below bulk T_c or continuously evolved into SC gap. Even though such a smooth dI/dV evolution across T_c also has been widely observed in high-T_c cuprates, the origin of pseudogap still awaits an answer [39]. Taken together with a theoretical explanation that pseudogap behavior in STS of $CeCoIn_5$ can be explained using an electronic structure of heavy quasiparticle, the pseudogap in $CeCoIn_5$ is also controversial [47]. We finally note that several recent STS studies emphasized the importance of $c-f$ entanglement on the pseudogap development in $CeCoIn_5$, as is our study (see Fig. S6 in the Supplemental Material [20]) [9,17].

In summary, the f electron delocalization and the nature of pseudogap in $CeCoIn_5$ have been studied via energy-resolved spectroscopy and systematic pressure control. The evolution of dI/dV reveals the Fano asymmetry even at temperatures much higher than the transport Kondo coherence temperature, T_{coh}. Signifying the onset of itinerant heavy quasiparticles at T_{sat}, the Fano asymmetry under pressure shows a scaling behavior as a function of the reduced temperature of T/T_{sat} in the high-T regime. With decreasing temperature, a dip feature in dI/dV is observed around the zero-bias voltage in the normal state owing to the opening of the pseudogap. Applied pressure gradually increases both the pseudogap width Δ_g and onset temperature T_g, which is opposite of the pressure dependence of the SC gap, but is similar to that of T_{coh}. These discoveries underline that the origin of the pseudogap in $CeCoIn_5$ is not related to the formation of SC Cooper pairs, but arises from the collective Kondo hybridization effects. The successful demonstration of the energy-dependent transport spectroscopy under pressure is not only pertinent to the analysis of the pseudogap in the quantum critical compound $CeCoIn_5$, but is also expected to play a pivotal role in elucidating the origin of pseudogap and their connection to superconductivity in other families of unconventional superconductors, such as high-T_c cuprates.

We acknowledge fruitful discussion with J. D. Thompson and W. K. Park. This work was supported by the National Research Foundation (NRF) of Korea through a grant funded by the Korean Ministry of Science and ICT (No. 2021R1A2C2010925). Work at Zhejiang University was supported by the National Key Research and Development Program of China (No. 2017YFA0303101).

*tp8701@skku.edu

[1] E. J. Mueller, Review of pseudogaps in strongly interacting Fermi gases, Rep. Prog. Phys. **80**, 104401 (2017).
[2] W.-L. Tu and T.-K. Lee, Evolution of pairing orders between pseudogap and superconducting phases of cuprate superconductors, Sci. Rep. **9**, 1719 (2019).
[3] M. Vojta, Lattice symmetry breaking in cuprate superconductors: Stripes, nematics, and superconductivity, Adv. Phys. **58**, 699 (2009).
[4] N. Doiron-Leyraud, O. Cyr-Choinière, S. Badoux, A. Ataei, C. Collignon, A. Gourgout, S. Dufour-Beauséjour, F. F. Tafti, F. Laliberté, M. E. Boulanger, M. Matusiak, D. Graf, M. Kim, J. S. Zhou, N. Momono, T. Kurosawa, H. Takagi, and L. Taillefer, Pseudogap phase of cuprate superconductors confined by Fermi surface topology, Nat. Commun. **8**, 2044 (2017).
[5] J. Merino and O. Gunnarsson, Pseudogap and singlet formation in organic and cuprate superconductors, Phys. Rev. B **89**, 245130 (2014).
[6] M. Frachet, I. Vinograd, R. Zhou, S. Benhabib, S. Wu, H. Mayaffre, S. Krämer, S. K. Ramakrishna, A. P. Reyes, J. Debray, T. Kurosawa, N. Momono, M. Oda, S. Komiya, S. Ono, M. Horio, J. Chang, C. Proust, D. LeBoeuf, and M.-H. Julien, Hidden magnetism at the pseudogap critical point of a cuprate superconductor, Nat. Phys. **16**, 1064 (2020).
[7] K. B. Efetov, H. Meier, and C. Pépin, Pseudogap state near a quantum critical point, Nat. Phys. **9**, 442 (2013).
[8] S. Badoux, W. Tabis, F. Laliberté, G. Grissonnanche, B. Vignolle, D. Vignolles, J. Béard, D. A. Bonn, W. N. Hardy, R. Liang, N. Doiron-Leyraud, L. Taillefer, and C. Proust, Change of carrier density at the pseudogap critical point of a cuprate superconductor, Nature (London) **531**, 210 (2016).
[9] B. B. Zhou, S. Misra, E. H. da Silva Neto, P. Aynajian, R. E. Baumbach, J. D. Thompson, E. D. Bauer, and A. Yazdani, Visualizing nodal heavy fermion superconductivity in $CeCoIn_5$, Nat. Phys. **9**, 474 (2013).
[10] H. Murayama, Y. Sato, R. Kurihara, S. Kasahara, Y. Mizukami, Y. Kasahara, H. Uchiyama, A. Yamamoto, E. G. Moon, J. Cai, J. Freyermuth, M. Greven, T. Shibauchi, and Y. Matsuda, Diagonal nematicity in the

pseudogap phase of $HgBa_2CuO_{4+\delta}$, Nat. Commun. **10**, 3282 (2019).

[11] Y. Xu, P. Richard, K. Nakayama, T. Kawahara, Y. Sekiba, T. Qian, M. Neupane, S. Souma, T. Sato, T. Takahashi, H. Luo, H. Wen, G. Chen, N. Wang, Z. Wang, Z. Fang, X. Dai, and H. Ding, Fermi surface dichotomy of the superconducting gap and pseudogap in underdoped pnictides, Nat. Commun. **2**, 392 (2011).

[12] S. Kawasaki, M. Yashima, T. Mito, Y. Kawasaki, G. q. Zheng, Y. Kitaoka, D. Aoki, Y. Haga, and Y. Ōnuki, The phase diagram of antiferromagnetism and superconductivity in $CeRhIn_5$: A study of ^{115}In NQR under pressure, J. Phys. Condens. Matter **17**, S889 (2005).

[13] B. J. Powell, E. Yusuf, and R. H. McKenzie, Spin fluctuations and the pseudogap in organic superconductors, Phys. Rev. B **80**, 054505 (2009).

[14] T. Timusk and B. Statt, The pseudogap in high-temperature superconductors: An experimental survey, Rep. Prog. Phys. **62**, 61 (1999).

[15] S. Wirth, Y. Prots, M. Wedel, S. Ernst, S. Kirchner, Z. Fisk, J. D. Thompson, F. Steglich, and Y. Grin, Structural investigations of $CeIrIn_5$ and $CeCoIn_5$ on macroscopic and atomic length scales, J. Phys. Soc. Jpn. **83**, 061009 (2014).

[16] V. A. Sidorov, M. Nicklas, P. G. Pagliuso, J. L. Sarrao, Y. Bang, A. V. Balatsky, and J. D. Thompson, Superconductivity and Quantum Criticality in $CeCoIn_5$, Phys. Rev. Lett. **89**, 157004 (2002).

[17] A. Gyenis, B. E. Feldman, M. T. Randeria, G. A. Peterson, E. D. Bauer, P. Aynajian, and A. Yazdani, Visualizing heavy fermion confinement and Pauli-limited superconductivity in layered $CeCoIn_5$, Nat. Commun. **9**, 549 (2018).

[18] Y. Song, W. Wang, J. S. Van Dyke, N. Pouse, S. Ran, D. Yazici, A. Schneidewind, P. Čermák, Y. Qiu, M. B. Maple, D. K. Morr, and P. Dai, Nature of the spin resonance mode in $CeCoIn_5$, Commun. Phys. **3**, 98 (2020).

[19] M. Nicklas, R. Borth, E. Lengyel, P. G. Pagliuso, J. L. Sarrao, V. A. Sidorov, G. Sparn, F. Steglich, and J. D. Thompson, Response of the heavy-fermion superconductor $CeCoIn_5$ to pressure: Roles of dimensionality and proximity to a quantum-critical point, J. Phys. Condens. Matter **13**, L905 (2001).

[20] See Supplemental Material http://link.aps.org/supplemental/10.1103/PhysRevLett.130.076301 for the details in experimental methods (Sec. A), junction diagnostics (Sec. B), Fano resonance model (Sec. C), spectra reproducibility, and more (Sec. D), which includes Refs. [21–33].

[21] A. M. Duif, A. G. M. Jansen, and P. Wyder, Point-contact spectroscopy, J. Phys. Condens. Matter **1**, 3157 (1989).

[22] Y. G. Naidyuk and I. K. Yanson, PCS of superconductors, in *Point-Contact Spectroscopy*, edited by Y. G. Naidyuk and I. K. Yanson (Springer New York, 2005), pp. 193.

[23] G. Wexler, The size effect and the non-local Boltzmann transport equation in orifice and disk geometry, Proc. Phys. Soc. London **89**, 927 (1966).

[24] P. Coleman, Heavy fermions: Electrons at the edge of magnetism, *Handbook of Magnetism and Advanced Magnetic Materials* (Wiley Online Library, New York, 2007).

[25] J. Gramich, P. Brenner, C. Sürgers, H. v. Löhneysen, and G. Goll, Experimental verification of contact-size estimates in point-contact spectroscopy on superconductor/ferromagnet heterocontacts, Phys. Rev. B **86**, 155402 (2012).

[26] D. Gall, Electron mean free path in elemental metals, J. Appl. Phys. **119**, 085101 (2016).

[27] S. Zhang, G. Chappell, N. Pouse, R. E. Baumbach, M. B. Maple, L. H. Greene, and W. K. Park, Origin of gaplike behaviors in URu_2Si_2: Combined study via quasiparticle scattering spectroscopy and resistivity measurements, Phys. Rev. B **102**, 081101(R) (2020).

[28] Y. Onose, N. P. Ong, and C. Petrovic, The Lorenz number in $CeCoIn_5$ inferred from the thermal and charge Hall currents, Europhys. Lett. **80**, 37005 (2007).

[29] U. Fano, Effects of configuration interaction on intensities and phase shifts, Phys. Rev. **124**, 1866 (1961).

[30] V. Madhavan, W. Chen, T. Jamneala, M. F. Crommie, and N. S. Wingreen, Tunneling into a single magnetic atom: Spectroscopic evidence of the Kondo resonance, Science **280**, 567 (1998).

[31] K. Nagaoka, T. Jamneala, M. Grobis, and M. F. Crommie, Temperature Dependence of a Single Kondo Impurity, Phys. Rev. Lett. **88**, 077205 (2002).

[32] P. W. Anderson, Localized magnetic states in metals, Phys. Rev. **124**, 41 (1961).

[33] M. P. Allan, F. Massee, D. K. Morr, J. Van Dyke, A. W. Rost, A. P. Mackenzie, C. Petrovic, and J. C. Davis, Imaging cooper pairing of heavy fermions in $CeCoIn_5$, Nat. Phys. **9**, 468 (2013).

[34] Y.-f. Yang, Fano effect in the point contact spectroscopy of heavy-electron materials, Phys. Rev. B **79**, 241107(R) (2009).

[35] M. Maltseva, M. Dzero, and P. Coleman, Electron Cotunneling into a Kondo Lattice, Phys. Rev. Lett. **103**, 206402 (2009).

[36] M. Fogelström, M. J. Graf, V. A. Sidorov, X. Lu, E. D. Bauer, and J. D. Thompson, Two-channel point-contact tunneling theory of superconductors, Phys. Rev. B **90**, 104512 (2014).

[37] G. E. Blonder, M. Tinkham, and T. M. Klapwijk, Transition from metallic to tunneling regimes in superconducting microconstrictions: Excess current, charge imbalance, and supercurrent conversion, Phys. Rev. B **25**, 4515 (1982).

[38] W. K. Park, J. L. Sarrao, J. D. Thompson, and L. H. Greene, Andreev Reflection in Heavy-Fermion Superconductors and Order Parameter Symmetry in $CeCoIn_5$, Phys. Rev. Lett. **100**, 177001 (2008).

[39] Ø. Fischer, M. Kugler, I. Maggio-Aprile, C. Berthod, and C. Renner, Scanning tunneling spectroscopy of high-temperature superconductors, Rev. Mod. Phys. **79**, 353 (2007).

[40] Y.-f. Yang and D. Pines, Universal Behavior in Heavy-Electron Materials, Phys. Rev. Lett. **100**, 096404 (2008).

[41] C. Petrovic, P. G. Pagliuso, M. F. Hundley, R. Movshovich, J. L. Sarrao, J. D. Thompson, Z. Fisk, and P. Monthoux, Heavy-fermion superconductivity in $CeCoIn_5$ at 2.3 K, J. Phys. Condens. Matter **13**, L337 (2001).

[42] S. Nakatsuji, D. Pines, and Z. Fisk, Two Fluid Description of the Kondo Lattice, Phys. Rev. Lett. **92**, 016401 (2004).

[43] S. Jang, J. D. Denlinger, J. W. Allen, V. S. Zapf, M. B. Maple, J. N. Kim, B. G. Jang, and J. H. Shim, Evolution of the Kondo lattice electronic structure above the transport

coherence temperature, Proc. Natl. Acad. Sci. U.S.A. **117**, 23467 (2020).

[44] Q. Y. Chen, D. F. Xu, X. H. Niu, J. Jiang, R. Peng, H. C. Xu, C. H. P. Wen, Z. F. Ding, K. Huang, L. Shu, Y. J. Zhang, H. Lee, V. N. Strocov, M. Shi, F. Bisti, T. Schmitt, Y. B. Huang, P. Dudin, X. C. Lai, S. Kirchner, H. Q. Yuan, and D. L. Feng, Direct observation of how the heavy-fermion state develops in $CeCoIn_5$, Phys. Rev. B **96**, 045107 (2017).

[45] K. Kummer, S. Patil, A. Chikina, M. Güttler, M. Höppner, A. Generalov, S. Danzenbächer, S. Seiro, A. Hannaske, C. Krellner, Y. Kucherenko, M. Shi, M. Radovic, E. Rienks, G. Zwicknagl, K. Matho, J. W. Allen, C. Laubschat, C. Geibel, and D. V. Vyalikh, Temperature-Independent Fermi Surface in the Kondo Lattice $YbRh_2Si_2$, Phys. Rev. X **5**, 011028 (2015).

[46] K. Shrestha, S. Zhang, L. H. Greene, Y. Lai, R. E. Baumbach, K. Sasmal, M. B. Maple, and W. K. Park, Spectroscopic evidence for the direct involvement of local moments in the pairing process of the heavy-fermion superconductor $CeCoIn_5$, Phys. Rev. B **103**, 224515 (2021).

[47] J. S. Van Dyke, J. C. S. Davis, and D. K. Morr, Differential conductance and defect states in the heavy-fermion superconductor $CeCoIn_5$, Phys. Rev. B **93**, 041107(R) (2016).